Original Research Article

Institution of MECHANICAL ENGINEERS
Journal of MECHANICAL ENGINEERING SCIENCE

Proc IMechE Part C:
J Mechanical Engineering Science
2022, Vol. 0(0) 1–8

DOI: 10.1177/09544062221112798
journals.sagepub.com/home/pic
SAGE

Mechanical properties of aluminum/SiNT nanocomposite

Mohsen Motamedi, Ali Mehrvar and Mohamadhossein Nikzad

Abstract

Molecular dynamics simulation is among the most significant methods in nanoscale studies. This paper studied the effect of strain rate, temperature, and nanotube chirality on the stress-strain behavior of aluminum/silicon nanotubes (SiNTs) using molecular dynamics simulation. Ultimate tensile stress and Young's modulus of the nanocomposite were evaluated using molecular dynamics simulation. According to the results, Young's modulus of the nanocomposite decreased with increasing temperature. Also, Young's modulus decreased by increasing the strain rate. Next, an experimental approach was used based on the Box–Behnken design. According to the input parameters and the experimental approach, the number of simulations in the software was 39 runs. Overall, it is concluded that the optimal conditions were created at a temperature of 50 K, a strain rate of 0.01/ps, and chirality of (5,5), leading to the elasticity modulus of 137 GPa and the ultimate tensile stress of 11.8 GPa.

Keywords

Molecular dynamics simulation, nanocomposites, young's modulus, stress-strain behavior, response surface methodology

Date received: 17 February 2022; accepted: 22 June 2022

Introduction

Today, silicon nanotubes (SiNTs) have found numerous applications such as in battery anodes,[1,2] lithium-ion batteries,[3] chemical sensors,[4] biosensing and bioimaging analysis,[5] ultralow-power logic applications,[6] and transistors.[7,8] Using the basic law of density function calculations, Singh et al.[9] indicated that hexagonal metal SiNT could be consolidated by condensation with three-dimensional metal atoms. Finished nanotubes with iron and manganese had high magnetic moments. Also, infinitely ferromagnetic $Si_{24}Fe_4$ nanotubes with localized magnetic moment were almost identical for each iron atom in bulk iron.

Silicon was used for electrodes in batteries (lithium-ion) because of its high energy density. Maintaining the weak capacity due to Si powdering during the cycle made its practical application disappointing. Song et al.[10] produced a nanostructured form of Si that could adapt to high charges in battery applications.

Le et al.[11] studied the basic properties of Si nanotubes and described their abilities to regulate the structure of a given SiNT through artificial control. Therapeutic metal nanoparticles were briefly described as experiments with the ability to internally load a given nanotube with species capable of delivering drugs by a magnetic field. Given the wide range of diverse features demonstrated to date, using SiNTs as therapeutic platforms is quite promising.

The molecular dynamics method is one of the best methods to simulate materials and study their properties. Among the cases studied in this regard are evaluating corrosion behavior of bulk nanocrystalline,[12] assessing the effect of straight and wavy carbon nanotubes (CNT) on the reinforcement modulus of nanocomposites,[13] exploring the effect of different parameters on the thermal conductivity of silicon and CNTs,[14] apprising mechanical properties of CNT junction,[15] and investigating different parameters on mechanical properties of SiNTs.[16]

Numerous molecular dynamics simulations have been performed on aluminum metal composites. For example, a molecular dynamics study was used to predict the deformation and failure of the aluminum-silicon interface.[17] In addition, the effect of different temperatures on the maximum shear stress of aluminum-graphene composite was studied using the molecular dynamics method.[18] In addition, Patel et al.[19] predicted the interfacial properties of aluminum single-walled carbon nanotube (SWCNT) composite using molecular dynamics.

The effects of CNT defects on the properties of aluminum-CNTs composites using mild and severe CNT damage were reviewed in by Hassan et al.[20] Composites prepared with lightly damaged CNTs had more than 90% strength and higher modulus than pure aluminum.

Department of Mechanical Engineering, Shahreza Campus, University of Isfahan, Isfahan, Iran

Corresponding author:
Mohsen Motamedi, Department of Mechanical Engineering, Shahreza Campus, University of Isfahan, Isfahan, Iran.
Email: motamedi@shahreza.ac.ir

The tensile test of CNT reinforced copper was evaluated by Yan et al.[21] using molecular dynamics simulation. Results showed that increasing the number of nanotubes, the diameter and the number of layers increased the elastic modulus of copper/CNTs composite.

So far, several studies have been conducted on the properties of aluminum and its compounds, such as studying the effect of heat transfer on suspended water by aluminum alloy nanomaterials,[22] the heat transfer on Al_2O_3–H_2O,[23] and Al_2O_3 and γAl_2O_3 nanomaterials on advanced heat transfer in H_2O.[24] However, no research has been done on the properties of the combination of aluminum and silicon, including the mechanical properties of this compound. Therefore, the present research aims to study the mechanical properties of aluminum-SiNT nanocomposite. Overall, the results can be effective in designing and fabricating aluminum compounds in the composite industry.

This research has two parts. In the first part, the mechanical properties of aluminum/SiNT nanocomposites are obtained by MD using LAMMPS software. Then, the effects of strain rate, temperature, and chirality on the behavior of the stress-strain curve are investigated. In the second part, nanocomposites are optimized using the experimental design method and three input parameters, namely, temperature, strain rate, and chirality. Eventually, the optimal values are obtained for the modulus of elasticity and ultimate tensile stress.

Computational approach

MD method

The MD calculation and simulation were performed using the representative volume element (RVE) of an Al-included SiNT. The Al box has 12,167 atoms. The SiNTs with different chiralities were used in Al matrix. All SiNTs have a length of 92.2 Å. The first, second, third, fourth, and fifth SiNTs have a zigzag (3,3) configuration with 288 atoms, zigzag (4,4) configuration with 384 atoms, zigzag (5,5) configuration with 480 atoms, zigzag (6,6) configuration with 576 atoms, and zigzag (7,7) configuration with 672 atoms.

Potentials function

Three types of interatomic potentials, Al/Al, Silicon/Silicon (for SiNT), and Al/Si, were used in this work.

For Silicon/Silicon bonds, the Tersoff potential was applied.[25]

EAM potential was used for the Al/Al interaction as follows[26,27]:

$$E_i = F_\alpha\left(\sum_{j\neq i}\rho_\beta(r_{ij})\right) + \frac{1}{2}\sum_{j\neq i}\phi_{\alpha\beta}(r_{ij}) \quad (1)$$

where r_{ij} is the distance of the atoms i and j, $\emptyset_{\alpha\beta}$ is a potential function in pairs, ρ_β is electron charge density, and F_α is an embedding function.

Also, Lennard–Jones potential was used for Al/Si interaction as follows:

$$E = 4\varepsilon\left[\left(\frac{\sigma}{r}\right)^{12} - \left(\frac{\sigma}{r}\right)^{6}\right] \quad (2)$$

where ε is the potential well, σ is the distance, and r is atoms distance.

Simulation terms and conditions

The system was equilibrated in 1 nanosecond, in 50, 100, 273, 300, 350, 400, 450, 500, 600 K with periodic boundary conditions.

In molecular dynamics simulation, the RVE was pulled in the axis with strain rates of $10^{-5}/ps$, $10^{-4}/ps$, $10^{-3}/ps$, $10^{-2}/ps$, $3{*}10^{-2}/ps$, $5{*}10^{-2}/ps$, $7{*}10^{-2}/ps$ and $9{*}10^{-2}/ps$. Figure 1 presents pulling process of Al/SiNT composite till fracturing.

Results and discussion

Investigating the effect of different parameters

Temperature effect. First, the effect of temperature on the stress-strain curve of aluminum-SiNT nanocomposite was investigated. For this purpose, temperatures of 50, 100, 273, 300, 350, 400, 450, 500, and 600 K were used in this simulation. The chirality of the SiNT (6,6) was also considered. The system pressure was 100 KPa, and the strain rate was 0.0001/ps. The stress-strain diagram is shown in Figure 2.

The elastic modulus value of the materials can be obtained using the slope of the stress-strain diagram in the linear region. The ultimate tensile stress value can also be obtained from the peak point of the stress-strain diagram. For the above values, the elastic modulus and the ultimate stress values were extracted and shown in Table 1.

According to the results, Young's modulus of the nanocomposite decreases with increasing temperature. This result is consistent with the results of Bayer's experimental work[28] and Singh's simulation work.[29]

Although no special trend is observed with increasing temperature for the ultimate tensile stress value, it is clear that at 50K, the stress-strain diagram will be more inclined due to the extreme brittleness of the material. Therefore, the ultimate stress of the material will be more than its ultimate stress under the ductile state.

Investigating the effect of strain rate. One of the most critical parameters in the tensile test is the strain rate. In general, the strain value is obtained from the following equation:

$$\epsilon(t) = \frac{L(t) - L_0}{L_0} \quad (3)$$

where L_0 is the original length and $L(t)$ is current length (time t). The strain rate is:

$$\dot{\epsilon}(t) = \frac{d\epsilon}{dt} = \frac{d}{dt}\left(\frac{L(t) - L_0}{L_0}\right) = \frac{1}{L_0}\frac{dL(t)}{dt} = \frac{v(t)}{L_0} \quad (4)$$

where $v(t)$ is the speed of ends moving.

Table 1. The elastic modulus and ultimate stress of Al/SiNT nanocomposite for various temperatures.

Temperature(K)	50	100	273	300	350	400	450	500	600
Elastic modulus (GPa)	180.07	172.5	161.04	158.88	155.04	152.87	150.05	147.63	144.1
Ultimate stress (GPa)	38.315	21.51	14.39	23.07	27.235	22.39	22.277	31.46	21.39

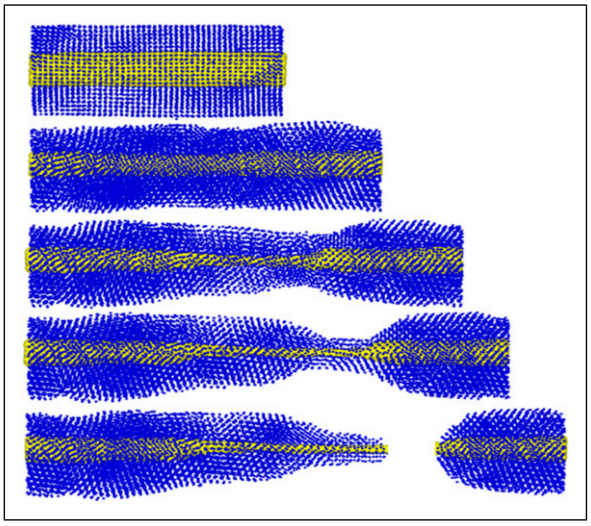

Figure 1. Pulling process of Al/SiNT composite till fracturing.

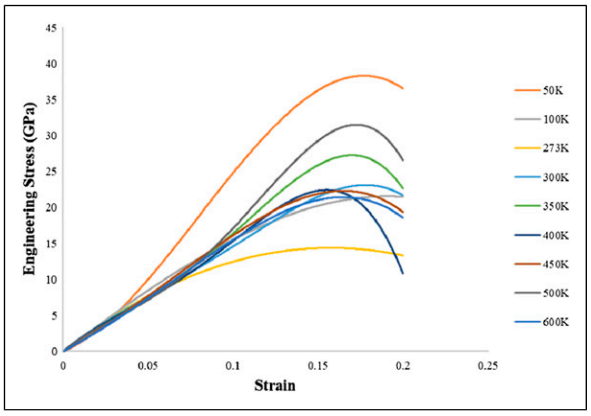

Figure 2. Effect of temperature on stress-strain diagram.

Figure 3 presents the stress-strain diagram of the nanocomposite for different strain rates. In this case, the chirality of the SiNT (6,6) is studied at a pressure of 100 KPa and at a temperature of 273 K.

The Young's modulus and the ultimate tensile stress of the nanocomposite are obtained from the stress-strain diagrams in Figure 3, the values of which are presented in Table 2.

As can be found in Figure 3 and Table 2, by increasing the strain rate from 0.00001/ps to 0.09/ps, Young's modulus decreased by 25%, which is a significant value. This result indicates that in molecular dynamics simulations, the strain rate parameter is one of the most significant and influential parameters in the results.

Jun Hua et al.[30] studied the effect of strain rate on the elastic modulus of Cu nanocomposite. The results showed that by increasing the strain rate from 0.0005/ps to 0.005/ps,

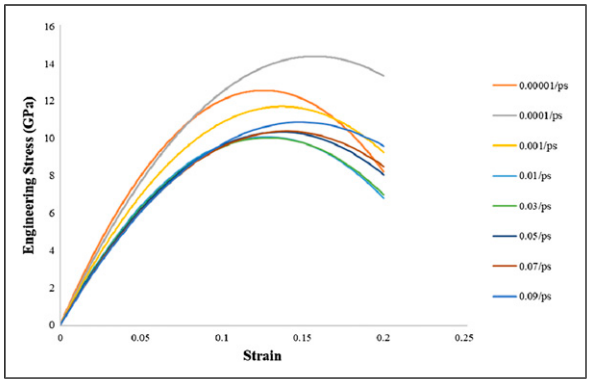

Figure 3. The stress-strain diagram of nanocomposite for different strain rates.

Young's modulus decreased from 210 GPa to 191 GPa (about 9%). In the present study, with the same order, if the strain rate changes from 0.0001/ps to 0.001/ps, Young's modulus will decrease by about 8%, indicating a good agreement. Also, Moeini et al.[31] indicated that an increase in the strain rate would decline Young's modulus of the nanocomposites.

Investigating the effect of chirality. Nanotubes with different chiralities were assessed to explore the effect of chirality on the properties of the nanocomposite. The chirality type of nanotubes is zigzag. Figure 4 illustrates the stress-strain diagram for the temperature of 273 K, the pressure of 100 KPa, and the stress rate of 0.01/ps. Also, Young's modulus and the ultimate stress for this case are shown in Table 3.

As expected, Young's modulus of nanocomposite declines by increasing chirality, which in turn increases the diameter. The reason is increasing the volume ratio of nanotubes in the composite due to the high strength of the nanotubes; therefore, it will have more significant effects on Young's modulus. According to the relationships between the composites, the volume of the composite V_{RVE} is represented as follows[32]:

$$V_{RVE} = V_{Al} + V_{SiNT} \tag{5}$$

Silvestre[32] used elasticity theory to predict composite elasticity is:

$$Y_{RVE} = V_{SiNT} Y_{SiNT} + V_{Al} Y_{Al} \tag{6}$$

Where V_{SiNT} and V_{Al} are volumes of SiNT and aluminum, respectively, and Y_{SiNT} and Y_{Al} are Young's moduli of SiNT and aluminum, respectively. It is clear that, as the volume percentage of nanotubes increases (which is due to the increase in chirality), Young's modulus increases as well.

Table 2. The elastic modulus and ultimate stress of Al/SiNT nanocomposite for different strain rates.

Strain Rate (1/ps)	0.00001	0.0001	0.001	0.01	0.03	0.05	0.07	0.09
Elastic modulus (GPa)	170.08	161.04	147.13	134.12	132.06	129.96	127.28	126.59
Ultimate stress (GPa)	12.572	14.39	11.7	10.082	10.036	10.324	10.382	10.85

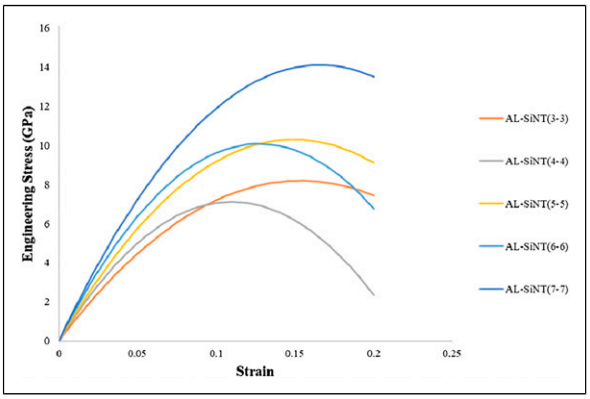

Figure 4. Effect of different chiralities on the stress-strain curve.

Table 3. The Young's modulus of Al/SiNT nanocomposite for different chiralities.

Chirality of SiNT (nm)	(3–3)	(4–4)	(5–5)	(6–6)	(7–7)
Elastic modulus (GPa)	93.138	106.34	119.98	134.12	150.29
Ultimate stress (GPa)	8.198	7.118	10.3	10.082	14.11

Table 4. Input parameters and their levels.

	Levels				
Input parameters	−2	−1	0	1	2
Temperature T (K)	50	200	350	500	650
Strain rate S (1/ps)	0.01	0.03	0.05	0.07	0.09
Chirality C (nm)	3 types: 1, 2 and 3				

Statistical modeling and optimization

In the design of experiments (DOEs), changes are consciously made in the process input variables to observe and identify the degree of changes in the output response of the process.[33,34] The procedure of this research is a combination of factors and parameters studied in the previous section, the output of which improves the mechanical properties. In this study, temperature, strain rate, and chirality were considered the input parameters while ultimate stress (Sut) and the Young's modulus (E) were considered the output parameters. Also, response surface methodology (RSM) was used as a DOE method, and MINITAB software was used to run the simulations.

The experimental strategy was used based on the Box–Behnken design. The temperature and strain rate parameters were considered in five levels, and the chirality parameters were considered in three types. Input parameters and their levels are presented in Table 4. According to the number of inputs and the experimental strategy, the number of simulation runs in the software is 39. Chiralities of (3,3), (4,4), and (5,5) refer to types 1, 2, and 3, respectively.

Table 5 presents the values of response variables for the 39 numerical simulations.

The mathematical modeling of the ultimate stress using the RSM. The quadratic mathematical model in terms of encoded input parameters for the response variable of the ultimate stress is as follows:

$$\begin{aligned}
\text{Sut} &= 10.288 - 0.008303\ \text{T} - 14.39\ \text{S} \\
&\quad + 0.000005\ \text{T*T} + 9.0\ \text{S*S} + 0.00694\ \text{T*S} \\
\text{Sut} &= 8.908 - 0.007415\ \text{T} - 12.20\ \text{S} \\
&\quad + 0.000005\ \text{T*T} + 9.0\ \text{S*S} + 0.00694\ \text{T*S} \\
\text{Sut} &= 12.446 - 0.008755\ \text{T} - 13.68\ \text{S} \\
&\quad + 0.000005\ \text{T*T} + 9.0\ \text{S*S} + 0.00694\ \text{T*S}
\end{aligned} \tag{7}$$

where T is the temperature (K), S is the strain rate in picoseconds, and Sut is the ultimate stress in GPa. The above three equations are for chiralities type 1 to type 3, respectively. As can be seen in equation (7), the ultimate stress values for each chirality can be obtained as a function of strain rate (S) and temperature (T).

The mathematical modeling of Young's modulus using the RSM. The mathematical model of Young's modulus is given in equation (8):

$$\begin{aligned}
\text{E} &= 116.57 - 0.09729\ \text{T} - 160.2\ \text{S} + 0.000056\ \text{T*T} \\
&\quad + 116\ \text{S*S} + 0.0754\ \text{T*S} \\
\text{E} &= 130.28 - 0.10099\ \text{T} - 169.3\ \text{S} + 0.000056\ \text{T*T} \\
&\quad + 116\ \text{S*S} + 0.0754\ \text{T*S} \\
\text{E} &= 144.30 - 0.10386\ \text{T} - 157.6\ \text{S} + 0.000056\ \text{T*T} \\
&\quad + 116\ \text{S*S} + 0.0754\ \text{T*S}
\end{aligned} \tag{8}$$

where T is the temperature (K), S is the strain rate in picoseconds, and E is Young's modulus in GPa. As can be seen in equation (8), Young's modulus values for each chirality can be obtained as a function of strain rate and temperature.

The effect of inputs on the ultimate stress and the Young's modulus. According to equation (7), the linear and quadratic terms obtained for the ultimate stress have the greatest effect on this output. In fact, according to the analysis of variance (ANOVA) results and considering *p*-value and F-value, linear terms and quadratic terms of temperature, and linear terms of chirality have the greatest impact on the ultimate stress. Figure 5 shows that the

Table 5. The values of response variables.

	Temperature	Strain rate	Chirality (3 types)	Elastic modulus	Ultimate stress
Run Order	T (K)	S (1/ps)	C (nm)	E (GPa)	Sut (GPa)
1	350	0.05	1	83.382	7.381
2	500	0.03	3	103.48	8.947
3	650	0.05	2	83.727	5.655
4	350	0.05	2	94.981	6.415
5	650	0.05	1	72.475	6.41
6	350	0.05	1	83.382	7.381
7	350	0.09	3	105.32	9.105
8	350	0.05	1	83.382	7.381
9	500	0.07	1	74.93	6.633
10	350	0.01	2	100.46	6.786
11	350	0.05	3	108.55	9.385
12	50	0.05	3	131.48	11.368
13	350	0.05	3	108.55	9.385
14	350	0.05	3	108.55	9.385
15	200	0.07	3	116.25	10.051
16	200	0.03	1	95.554	8.458
17	350	0.05	3	108.55	9.385
18	350	0.01	3	114.26	9.879
19	500	0.07	2	83.752	5.657
20	350	0.09	2	90.521	6.114
21	350	0.05	2	94.981	6.415
22	350	0.09	1	76.918	6.8
23	350	0.05	1	83.382	7.381
24	200	0.07	2	102.41	6.917
25	350	0.05	2	94.981	6.415
26	500	0.03	1	76.918	6.809
27	350	0.05	2	94.981	6.415
28	500	0.03	2	89.778	6.064
29	200	0.07	1	89.591	7.93
30	500	0.07	3	97.646	8.442
31	350	0.05	3	108.55	9.385
32	650	0.05	3	95.152	8.227
33	50	0.05	1	104.42	9.243
34	50	0.05	2	117.2	7.916
35	350	0.05	2	94.981	6.415
36	200	0.03	3	121.24	10.482
37	350	0.01	1	87.603	7.775
38	200	0.03	2	108.02	7.296
39	350	0.05	1	83.382	7.381

ultimate stress increases with increasing the strain rate, decreasing temperature, and considering a type-3 chirality.

According to equation (8) related to Young's modulus, linear terms, quadratic, and overlap of input parameters are effective. According to the *p*-value and F-value obtained from the ANOVA, the linear terms of temperature, chirality, and strain rate have the greatest effect on Young's modulus, in the order of their appearance. The quadratic terms of temperature and the interaction between temperature and chirality also affected Young's modulus. Furthermore, according to Figure 6, low temperatures, and low strain rates, and type-3 chirality increase Young's modulus.

Optimization with the desirability approach. Derringer et al.[35] developed this approach as a useful search-based optimization method to find the optimal solutions globally. In this approach, each individual desirability function is assigned between 1 and 0 for the outputs. Here, 1 indicates that the output is in full desirability and at its target, and 0 shows that the output is at the lowest desirability level.[36,37] Therefore, the purpose is to determine the values of the input variables for each output with desirability of greater than 0, and maximize the overall desirability. The purpose of optimization in this research is to maximize the ultimate stress and Young's modulus. The optimal parameters for simultaneous optimization of two response outputs are determined using the Derringer method. The result was obtained using Minitab software, shown in Figure 7. In this figure, the first row indicates the input parameters, the range of their changes, and the optimal value of the parameter between its upper and lower limits. Also, the first column represents the overall objective function, the objective

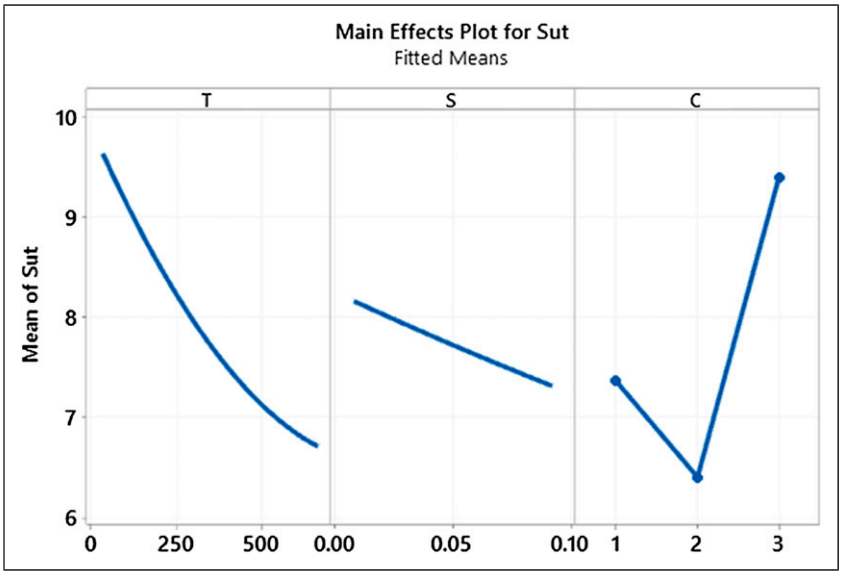

Figure 5. Effect of temperature, strain rate and chirality on ultimate stress.

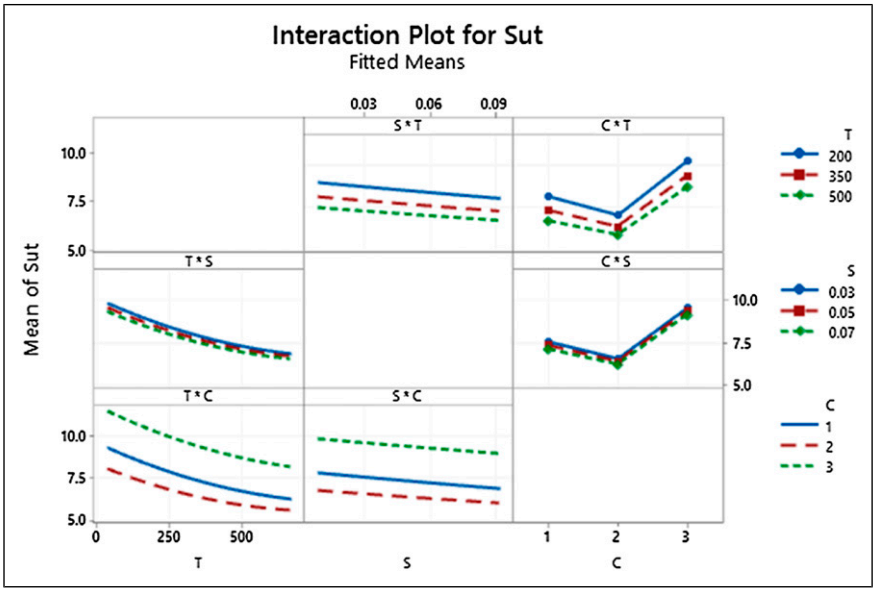

Figure 6. Interaction plot between temperature, strain rate and chirality on ultimate stress.

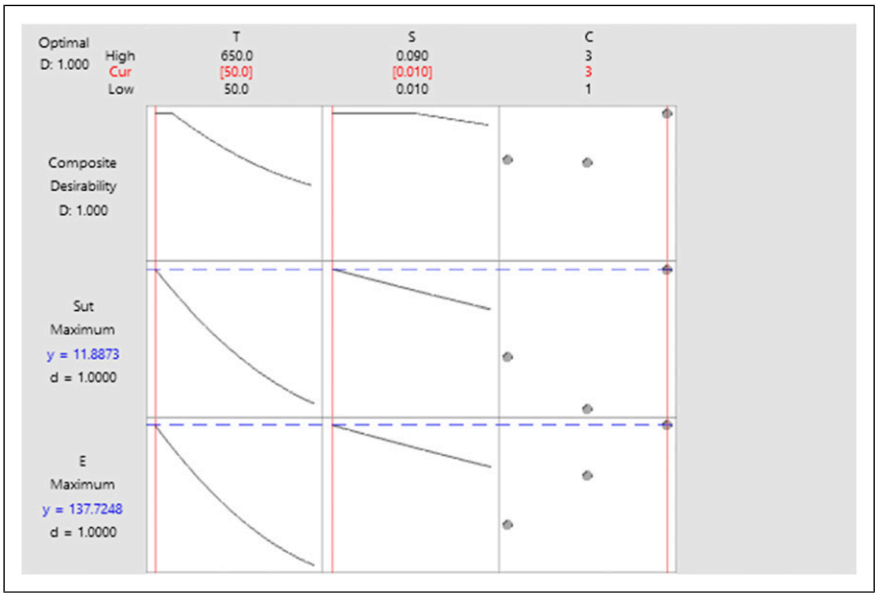

Figure 7. The optimal ultimate stress and Young's modulus Using the Derringer method.

Table 6. Optimal solution for parameters and responses.

Temp. (K)	Strain rate (1/ps)	Chirality	Sut (MPa)	E (GPa)
50	0.01	3	11.8873	137.725

function of each response variable, and the optimal value of the response variable. In addition, each cell in the figure describes how the response variable changes with respect to the change of one parameter while the other parameters are stable. In addition, in Figure 7, the red vertical line in each cell denotes the value of the optimal input parameter, and the blue dashed line shows the value of the optimal response variable. It can be concluded that the optimal conditions are created simultaneously at 50 K, a strain rate of 0.01/ps, and a third-type chirality (Table 6).

Conclusion

In this study, the mechanical properties of AL/SiNT nanocomposite were investigated. Next, we studied the effects of temperature change, strain rate, and chirality of nanotubes on the elastic modulus and the ultimate stress of the nanocomposite. The results indicated that Young's modulus decreases as temperature rises, but the ultimate stress does not show a specific trend. Afterward, the experimental design method was used to optimize and simultaneously study the effect of these 3 parameters on the properties of nanocomposites to find an optimal point for the elastic modulus and ultimate stress. Using the Derringer method, the optimal parameters for simultaneous optimization of two response variables (i.e., elastic modulus and final stress) were determined. It can be concluded that the optimal conditions are created simultaneously at a temperature of 50 K, a strain rate of 0.01/ps, and chirality of (5,5), leading to the elastic modulus of 137 GPa and the ultimate stress value of 11.8 GPa.

Authors' contributions

All authors contributed to the design and implementation of the research, to the analysis of the results and to the writing of the manuscript.

Declaration of Conflicting Interests

The author(s) declared no potential conflicts of interest with respect to the research, authorship, and/or publication of this article.

Funding

The author(s) received no financial support for the research, authorship, and/or publication of this article.

Availability of data and material

The data that support the findings of this study are available from the corresponding author

Code availability

The LAMMPS package is free and open-source software.

ORCID iDs

Mohsen Motamedi https://orcid.org/0000-0003-3296-4253
Ali Mehrvar https://orcid.org/0000-0003-0138-3632

References

1. Park MH, Kim MG, Joo J, et al. Silicon nanotube battery anodes. *Nano Lett* 2009; 9(11): 3844–3847.
2. Wu H, Chan G, Choi JW, et al. Stable cycling of double-walled silicon nanotube battery anodes through solid–electrolyte interphase control. *Nat Nanotechnol* 2012; 7(5): 310–315.
3. Chou SL, Zhao Y, Wang JZ, et al. Silicon/single-walled carbon nanotube composite paper as a flexible anode material for lithium ion batteries. *The J Phys Chem C* 2010; 114(37): 15862–15867.
4. Li K, Wang W and Cao D. Novel chemical sensor for CO and NO: silicon nanotube. *The J Phys Chem C* 2011; 115(24): 12015–12022.
5. Ji X, Wang H, Song B, et al. Silicon nanomaterials for biosensing and bioimaging analysis. *Front Chem* 2018; 6, 38. DOI: 10.3389/fchem.2018.00038
6. Fahad HM and Hussain MM. High-performance silicon nanotube tunneling FET for ultralow-power logic applications. *IEEE Transac Electron Devic* 2013; 60(3): 1034–1039.
7. Cui Y, Zhong Z, Wang D, et al. High performance silicon nanowire field effect transistors. *Nano Lett* 2003; 3(2): 149–152.
8. Wang D, Wang Q, Javey A, et al. Germanium nanowire field-effect transistors with SiO 2 and high-κ HfO 2 gate dielectrics. *Appl Phys Lett* 2003; 83(12): 2432–2434.
9. Singh AK, Briere TM, Kumar V, et al. Magnetism in transition-metal-doped silicon nanotubes. *Phys Rev Lett* 2003; 91(14): 146802.
10. Song T, Xia J, Lee JH, et al. Arrays of sealed silicon nanotubes as anodes for lithium ion batteries. *Nano Lett* 2010; 10(5): 1710–1716.
11. Le NT, Tian Y, Gonzalez-Rodriguez R, et al. Silicon nanotubes as potential therapeutic platforms. *Pharmaceutics* 2019; 11(11): 571.
12. Eskandari M, Yeganeh M and Motamedi M (2012). Investigation in the corrosion behaviour of bulk nanocrystalline 316L austenitic stainless steel in NaCl solution. *Micro Nano Lett* 2012; 7(4): 380–383.
13. Motamedi M, Eskandari M and Yeganeh M. Effect of straight and wavy carbon nanotube on the reinforcement modulus in nonlinear elastic matrix nanocomposites. *Mater Des* 2012; 34: 603–608.
14. Motamedi M, Safdari E and Nikzad M. Effect of different parameters on the heat transfer coefficient of silicon and carbon nanotubes. *Int Commun Heat Mass Transfer* 2021; 129: 105692.
15. Motamedi M, Mashhadi MM and Rastgoo A. Vibration behavior and mechanical properties of carbon nanotube junction. *J Comput Theor Nanosci* 2013; 10(4): 1033–1037.
16. Motamedi M and Safdari E. Effect of Diameter, Length, and Chirality on the Properties of Silicon Nanotubes. *Silicon* 2021: 1–8. DOI: 10.1007/s12633-021-01332-9
17. Ward DK, Curtin WA and Qi Y. Aluminum–silicon interfaces and nanocomposites: a molecular dynamics study. *Compos Sci Technol* 2006; 66(9): 1151–1161.

18. Jiang WG, Wu Y, Qin QH, et al. A molecular dynamics based cohesive zone model for predicting interfacial properties between graphene coating and aluminum. *Comput Mater Sci* 2018; 151: 117–123.
19. Patel PR, Sharma S and Tiwari SK. Molecular dynamics simulation for interfacial properties of carbon nanotube reinforced aluminum composites. *Model Simul Mater Sci Eng* 2020; 29(1): 015004.
20. Hassan MT, Esawi AM and Metwalli S. Effect of carbon nanotube damage on the mechanical properties of aluminium–carbon nanotube composites. *J Alloys Compounds* 2014; 607: 215–222.
21. Yan Y, Lei Y and Liu S. Tensile responses of carbon nanotubes-reinforced copper nanocomposites: molecular dynamics simulation. *Comput Mater Sci* 2018; 151: 273–277.
22. Adnan SZA, Khan U, Ahmed N, et al. Heat transfer enhancement in H2O suspended by aluminium alloy nanoparticles over a convective stretching surface. *Adv Mech Eng* 2020; 12(9): 1687814020942342.
23. Khan U, Ahmed N, Mohyud-Din ST, et al. Surface thermal investigation in water functionalized Al2O3 and γAl2O3 nanomaterials-based nanofluid over a sensor surface. *Appl Nanosci* 2020: 1–11. DOI: 10.1007/s13204-020-01527-3
24. Adnan, Khan U, Ahmed N, et al. Enhanced heat transfer in H2O inspired by Al2O3 and γAl2O3 nanomaterials and effective nanofluid models. *Adv Mech Eng* 2021; 13(5): 16878140211023604.
25. Tersoff J. Empirical interatomic potential for silicon with improved elastic properties. *Phys Rev B* 1988; 38(14): 9902–9905.
26. Winey JM, Kubota A and Gupta YM. A thermodynamic approach to determine accurate potentials for molecular dynamics simulations: thermoelastic response of aluminum. *Model Simul Mater Sci Eng* 2009; 17(5): 055004.
27. Winey JM, Kubota A and Gupta YM. Corrigendum on thermodynamic approach to determine accurate potentials for molecular dynamics simulations: thermoelastic response of aluminum. *Modell Simul Mater Sci Eng* 2010; 18: 029801.
28. Bayar S, Delale F and Liaw M Effect of temperature on mechanical properties of nanoclay-reinforced polymeric nanocomposites.I: experimental results. *J Aerosp Eng* 2014; 27: 491–504.
29. Singh A and KumarD. Effect of temperature on elastic properties of CNT-polyethylene nanocomposite and its interface using MD simulations. *J Mol Model* 2018; 24: 178.
30. Hua A, Duan Z, Song C, et al. Molecular dynamics study on the tensile properties of graphene/Cu nanocomposite. *Int J Comput Mater Sci Eng* 2017; 6(2): 1750021 (15 pages).
31. Moeini R, Barbaz Isfahani R, Saber-Samandari S, et al Molecular dynamics simulations of the effect of temperature and strain rate on mechanical properties of graphene–epoxy nanocomposites. *Mol Simul* 2020; 46(6): 476.
32. Silvestre N, Faria B and Canongia JN. Compressive behavior of CNT-reinforced aluminum composites using molecular dynamics. *Compos Sci Technol* 2014; 90: 16–24.
33. Myers RH and Montgomery DC, *Response Surface methodology: process and product optimization using designed experiments*. New York: Wiley, 1995.
34. Mehrvar A, Basti A and Jamali A Inverse modelling of electrochemical machining process using a novel combination of soft computing methods. *Proc Imeche C: J Mech Eng Sci* 2020; 234(17): 3436–3446.
35. Derringer G and Suich R. Simultaneous optimization of several response variables. *J Qual Technol* 1980; 12: 214–219.
36. Castillo ED, Montgomery DC and Mc Carville DR. Modified desirability functions for multiple response optimizations. *J Qual Technol* 1996; 28(3): 337–345.
37. Mehrvar A, Basti A and Jamali A. Modelling and parameter optimization in electrochemical machining process: application of dual response surface-desirability approach. *Lat Am Appl Res* 2017; 47(4): 157–162.